MDPI

Article

A Hybrid Damper with Tunable Particle Impact Damping and Coulomb Friction

Muhammad Ayaz Akbar [1] , Wai-On Wong [1,*] and Emiliano Rustighi [2]

[1] Department of Mechanical Engineering, The Hong Kong Polytechnic University, Hong Kong SAR, China; muhammad-ayaz.akbar@connect.polyu.hk
[2] Industrial Engineering Department, University of Trento, 38122 Trento, Italy; emiliano.rustighi@unitn.it
[*] Correspondence: mmwowong@polyu.edu.hk

Abstract: A particle impact damper (PID) dissipates the vibration energy of a structure through impacts within the damper. The PID is not commonly used in practice mainly because of its low damping-to-mass ratio and the difficulty in achieving its optimal design due to its nonlinear characteristics. In contrast, a Coulomb friction damper (FD) can offer a higher damping force-to-mass ratio than other dampers, but it is also difficult to be controlled precisely due to its nonlinear characteristics and excessive frequency sensitivity regarding the resonant frequency. This paper examines a hybrid damper by combining a particle impact damper and a Coulomb friction damper (PID + FD) theoretically and experimentally. A theoretical model of the proposed damper is developed and tested numerically on a single-degree-of-freedom (SDOF) structure. The predicted results are validated by experimental tests on a prototype of the proposed damper. The damping force provided by the FD in the prototype can be varied by adjusting the normal force applied through a compression spring, while the vibration energy dissipation by the PID can be varied by changing the cavity size of the PID. A parametric analysis of the proposed hybrid damper has been performed. The proposed hybrid damper can reduce the maximum vibration amplitude of the SDOF primary structure by 66% and 43% compared with using the FD and PID only. The proposed damper is found to be effective over a wide range of excitation frequencies. Furthermore, the proposed hybrid damper achieves a similar vibration suppression performance to the traditional tuned mass damper (TMD) of a similar mass ratio. The proposed damper does not require an optimally tuned natural frequency and damping, unlike the TMD, and therefore it does not have the detuning problem associated with the TMD. In addition, the performance of the proposed damper is tested and compared with the TMD for random earthquake excitation data. Consequently, the proposed hybrid damper may be a simpler and better alternative to the TMD in passive vibration control applications.

Keywords: particle impact damper; passive vibration control; nonlinear damping; friction damper; hybrid damper

1. Introduction

A tuned mass damper (TMD) or dynamic vibration absorber (DVA) is a passive control device that can be tuned and mounted to a flexible structure to reduce its resonant vibration [1]. The TMD was invented nearly a century ago but is still not commonly used in practice for damping machine vibrations mainly due to the difficulties of achieving the optimal natural frequency and damping ratios of the TMD for its best performance of vibration damping to the primary structure [2–5]. When the natural frequency of the primary vibrating structure is changed, the TMD will be detuned and becomes ineffective in redirecting the vibration energy from the primary structure to the TMD itself [6–10].

On the other hand, the particle impact damper (PID) [11–13] is a relatively new kind of vibration damper that can damp down structural vibrations over a much wider frequency range than the TMD [14]. The PID can dissipate the vibration energy of the primary system

through impacts within the damper itself [15]. The PID does not have the detuning problem in controlling the response of the structures [16]. The effectiveness of the PID in harsh environmental conditions, simple installation requirements, less sensitivity to the direction of excitation [17], and other benefits give the PID numerous advantages over other passive vibration absorbers. Moreover, the PID is negligibly sensitive to oil contamination, does not add significant excessive external weight [18], and is usually insensitive to atmospheric temperature [19]. The PID is capable of damping vibrations due to different kinds of excitations [20]. Material wearing is less likely to happen in the PID, and the PID is a simple, affordable, and highly reliable device [21] that can be used for passive vibration control. A key aspect of the PID is that it can operate in multiple directions over a wide range of frequencies [22]. In addition to all these advantages, the PID is also not commonly used in practice mainly because of its low damping-to-mass ratio and the difficulty in achieving optimal design due to its nonlinear nature. The working principle of the PID relies on impacts with the primary structure and the amount of energy dissipation by impact can be increased by using a heavy particle but it can induce high local stress to the primary structure, leading to structural integrity and noise problems.

The high nonlinearity of the PID led to contradicting conclusions in various studies [23]. Fundamental work on the particle impact damper can be found in the article of Bapat and Sankar [24], where a basic single-unit model of a PID in free and forced vibrations is presented. The study concluded that mass ratio, the coefficient of restitution, and container size were the parameters that affected the performance of the PID [25]. In the study of Papalou [26], the performance of a PID under harmonic excitations was studied in various parametric combinations and the effect of fundamental parameters on the overall performance was presented. However, it was concluded that the exact mathematical model for such a damper could not be established due to many nonlinear phenomena. Furthermore, Cheng et al. [27] showed that the damping generated by the PID depended on the number of impacts when the particle and the primary mass were in opposite directions rather than on the total number of impacts. The performance of the PID was studied by considering the different surface properties of particles by Li et al. [28], and it was concluded that metallic particles were more efficient in dissipating the vibration energy. Several subsequent studies have supported the application-based analysis of PID performance [29–33]. Particle impact dampers were also studied to reduce railway vibrations by Jin [34] and concluded that the tuned particle damper outperformed the traditional TMD and could work at a broader frequency range. Badri et al. [35] tried to combine the PID with a viscous damper and proposed an improved hybrid damper.

Furthermore, friction dampers have a higher damping force-to-mass ratio than viscous dampers and they are low cost and compact in size. However, friction dampers are not as commonly used as viscous dampers because their design involves nonlinear dynamics. Stick-slip behaviors and nonlinearity associated with the FD are the major challenges to overcome [36]. The stick-slip phenomenon arises when the excitation force magnitude is not sufficient to overcome the static friction. A review of the available FD models is reported by Gagon et al. [37]. A steady-state solution of forced vibrations with a hybrid damper combining viscous and Coulomb dampers was derived by Den Hartog [38]. Considering the various challenges associated with the FD and ineffectiveness at resonance, it is usually combined with other dampers [39–44]. The FD can produce a large damping force and combining it with other suitable dampers could make the combination effective at resonance with various other advantages.

Overall, the PID and FD are two vibration suppression devices with advantages and disadvantages as discussed above. Theoretically, a friction damper is considered ineffective at resonance. However, various researchers have shown that the FD can reduce the damping peak in practical applications due to the presence of internal damping in structures. The stick-slip phenomenon can induce high-frequency vibrations in the structure, and the durability of the FD is reduced due to material removal and increased temperature [45]. In the case of large structure vibrations, global damping was also studied in [46]. Structural

vibration control usually requires a higher damping force to reduce the vibration amplitude of large structures. Therefore, the capability of the FD to produce a larger damping force can be useful if it can be made effective at resonance. On the other hand, the PID shows a low damping-to-mass ratio, requiring larger added mass to the primary system to achieve higher damping.

Therefore, a hybrid damper consisting of a PID and FD is proposed for the very first time, which utilizes the advantages of both damping technologies for the improvement of the damping capacity of the PID and FD. It is illustrated that the two dampers, the PID and FD, can supplement each other to avoid their respective constraints if designed properly and implemented according to the procedure established in this study. A numerical model is developed to simulate the hybrid damper effect on the response of an SDOF structure. Additionally, a parametric analysis of the hybrid damper has been carried out to formulate the optimal design methodology. A prototype of the hybrid damper is built to validate the numerical model and the numerical results.

2. Numerical Modelling and Experimental Validation

The numerical models of the particle impact damper (PID) and the proposed hybrid damper consisting of a PID and FD are established. The mechanical model of the SDOF structure with a particle impact damper is shown in Figure 1, where k is the spring constant and c represents the equivalent viscous damping coefficient of the system damping. The mass of the primary structure is denoted by M, while the mass of the particle is denoted by m. The particle can travel within a maximum distance of $2d$ and hit the primary structure when it reaches the boundary.
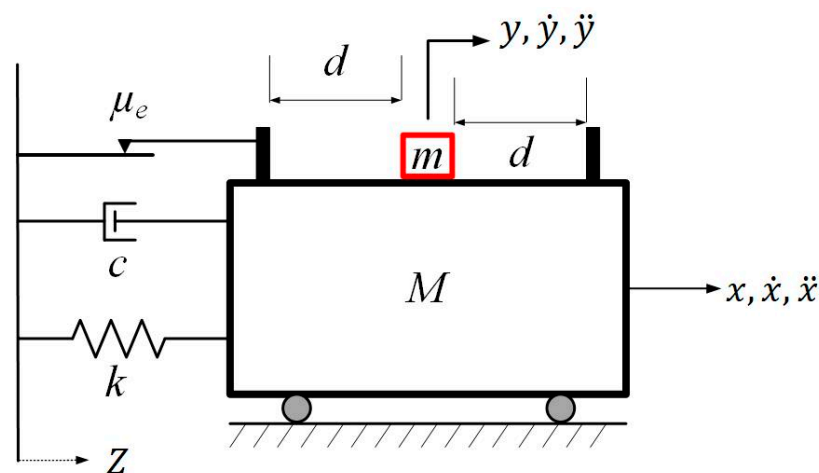
Figure 1. Mechanical model of a single-degree-of-freedom structure with the proposed hybrid damper.

Neglecting friction inside the PID, the equation of motion for the primary structure before any impact occurred may be written as

$$M\ddot{x} + c(\dot{x} - \dot{z}) + k(x - z) + F_f \text{sgn}(\dot{x} - \dot{z}) = 0 \tag{1}$$

Here, $F_f = \mu_e F_N$ is the friction force. The sgn is the signum function, which is defined as

$$\text{sgn}(\dot{x} - \dot{z}) = \begin{cases} -1 \text{ if } \dot{x} - \dot{z} < 0 \\ 0 \text{ if } \dot{x} - \dot{z} = 0 \\ 1 \text{ if } \dot{x} - \dot{z} > 0 \end{cases} \tag{2}$$

The equation of motion of the particle may be written as

$$m\ddot{y} = 0 \tag{3}$$

An impact occurs when the difference between the position of the primary mass and particle is equal to the clearance size, which can be expressed as

$$|x(t) - y(t)| \geq d \tag{4}$$

At each impact, energy is dissipated or redistributed depending on the direction of the particle and primary mass. Furthermore, the velocities of the particle and primary mass change at each impact. If the impact is perfectly elastic, the equation of the conservation of momentum can be utilized to determine the velocities of both objects after impact. The conservation of momentum between two colliding bodies is defined as

$$M\dot{x}_n^- + m\dot{y}_n^- = M\dot{x}_n^+ + m\dot{y}_n^+ \tag{5}$$

where $\left(\dot{x}_n^+, \dot{x}_n^-\right)$ and $\left(\dot{y}_n^+, \dot{y}_n^-\right)$ are the velocity vectors of the primary structure and particle before and after the nth impact. The superscript plus $(+)$ denotes the velocity after impact and minus $(-)$ denotes the velocity before impact. The conservation of momentum states that the impact is perfectly elastic and all the energy is conserved. However, most impacts are not perfectly elastic in practice. There will be some energy dissipated during the impact through material compression, heat, or other means. Therefore, the coefficient of restitution is the measure of energy dissipated during impacts calculated as the ratio of final to initial velocity difference. This may be written as

$$e = -\frac{\dot{x}_n^+ - \dot{y}_n^+}{\dot{x}_n^- - \dot{y}_n^-} \tag{6}$$

Hence, accurate calculation of the velocities after impact, in this case, must include the conservation of momentum and the coefficient of restitution. Therefore, combining and rearranging Equations (5) and (6) for the velocities of the particle and primary structure after each impact gives

$$\dot{x}_n^+ = \frac{\left[\left\{(1 - \beta e)\dot{x}_n^-\right\} + \left\{\beta(1 + e)\dot{y}_n^-\right\}\right]}{(1 + \beta)} \tag{7}$$

$$\dot{y}_n^+ = \frac{\left[\left\{(1 + e)\dot{x}_n^-\right\} + \left\{(\beta - e)\dot{y}_n^-\right\}\right]}{(1 + \beta)} \tag{8}$$

Here, $\beta = m/M$ is the mass ratio.

The numerical solution of the PID requires a time-based approach to identify the impacts accurately. The flowchart shows the computation principle in Figure 2. The Runge–Kutta fourth-order method is used to solve the equations of motion. The method begins with the vibration of the primary structure due to the support motion $z(t)$. The impact is then identified based on the condition $(|x(t) - y(t)| > d)$. The velocities after the impacts are calculated through Equations (5) and (6). Then the system restarts based on the calculated velocities and the position at the time of impact as initial conditions. If the condition for the impact is not satisfied, then the next time step is computed. A minimum time step is recommended for determining the precise impact time, although it may increase the computational effort. Generally, the parameters affecting the damping performance of PID [24,47] are clearance (d), the coefficient of restitution (e), and mass ratio (β). The mass ratio is fixed at 0.1 for the numerical simulations.
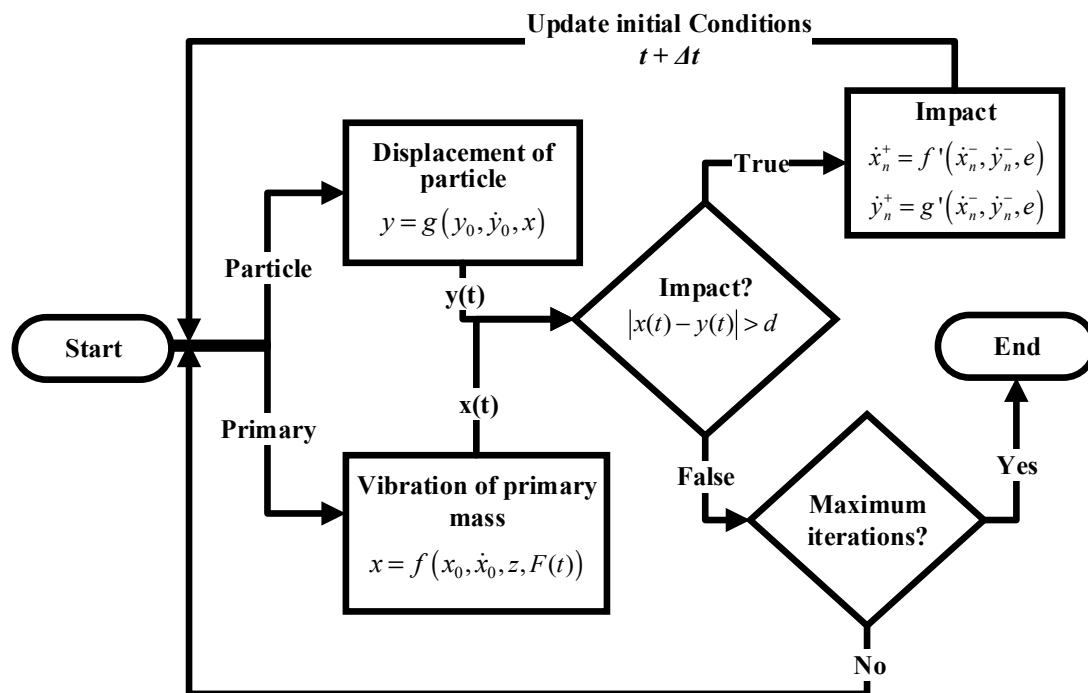
Figure 2. Process flow chart of the numerical model.

Experimental Identification of Model Parameters

The contact time between the particle and primary mass is neglected in the numerical models of the PID in the literature. The negligible contact time assumption may be acceptable if a large coefficient of restitution such as $e \approx 0.8$ is considered to represent a "hard" impact. However, some numerical tests using the present model show that the best damping performance of the PID can be achieved at a mid-range magnitude of the coefficient of restitution of about 0.5. A cushioning material (Polyurethane Foam) is therefore used in the proposed PID design to affirm the mid-range coefficient of restitution. To improve the accuracy of the proposed numerical model, the contact time and coefficient of restitution are determined by conducting experiments with a hard impact (steel-to-aluminum impact) and a soft impact (steel-to-foam impact), as shown in Figure 3.
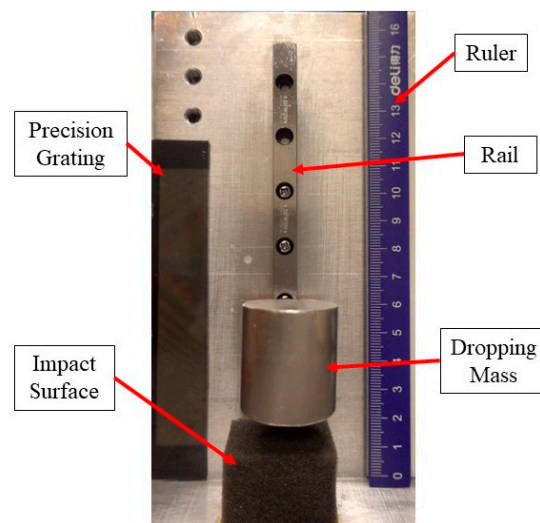
Figure 3. Experiment to determine the COR and contact time.

A particle made of mild steel is dropped fixed to a train (from the rail-train mechanism) from different heights, as shown in Figure 3. The experiment is recorded with a high-speed

camera (Sony RX100-M7) in a 20× slow-motion video with 1000 frames per sec. The frames are then extracted and analyzed to calculate the instant of contact between the particle and primary mass and the time of separation during the rebound to determine the contact time. A ruler together with a precision transmission grating (Sine Patterns LLC) is used in the experiment to provide the spatial reference of any image distortion due to the lens of the camera and the resolution. Similarly, the frames, each of 3456 × 2304 pixels, are extracted from the recorded videos and the frame with the release and final rebound height is processed in a CAD software program to calculate the coefficient of restitution. The impact velocity of the particle can be determined from the dropping height with gravitational acceleration. The COR is defined as $e = \frac{v_f}{v_i}$, and kinetic and potential energies are calculated as

$$\frac{1}{2}mv^2 = mgh$$

$$v = \sqrt{2gh}$$

Hence, substituting this in the coefficient of restitution expression gives

$$e = \frac{v_f}{v_i} = \frac{\sqrt{2gh_f}}{\sqrt{2gh_i}} = \sqrt{\frac{h_f}{h_i}} \tag{9}$$

The free-fall experiment is repeated three times, and the magnitude of the COR is calculated from Equation (9). The average magnitude of the COR for soft impact is measured as 0.47, and 0.82 for hard impact.

Determining the coefficient of restitution with different impact velocities justifies the assumption that the COR remains constant in each impact, as shown in Figure 4a. Similarly, the contact time during impact with different impact velocities is measured and plotted in Figure 4b. The average time determines the contact time between the particle and primary mass with a hard impact surface and cushioning material as presented in Table 1. The time step used in the numerical simulation is 0.001 s. The contact times between the colliding masses are added in all the numerical simulations presented in this paper. In addition, the COR is the measure of the impact surface in the numerical model; therefore, only two impact surfaces with a higher and lower COR are tested to study the effect of the COR on the damping performance. As mentioned, the hard aluminum impact surface is created without using any cushioning material. On the other hand, a commonly available cushioning material (PU foam) is fixed on the container wall for a soft impact with a lower COR.
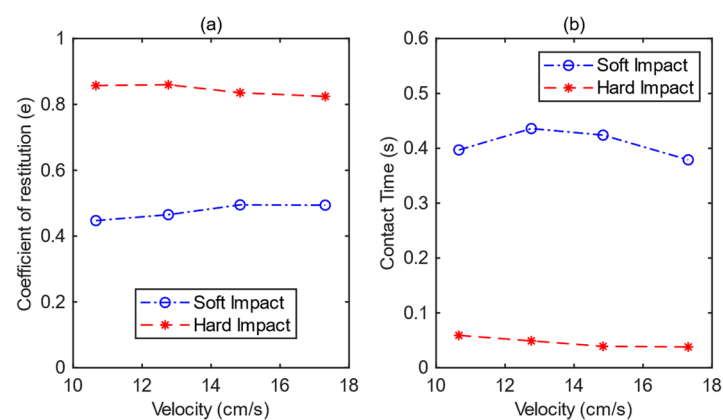
Figure 4. Measurement of coefficient of restitution of (**a**) hard (steel–aluminum), and (**b**) soft (steel–foam) surfaces with different impact velocities.

Table 1. Calculated contact time and coefficient of restitution of different types of impact surfaces used.

Hard/Soft Impact	Contact Time (s)	Coefficient of Restitution
Hard Impact (Steel–Aluminum)	0.046	0.82
Soft Impact (Steel–Foam)	0.411	0.47

3. Experimental Setup and Structural Parameters Identification

A prototype consisting of a single-degree-of-freedom structure is designed and tested with a PID, as shown in Figure 5. The experimental setup consists of a primary mass, contactless displacement sensors, an exciter, and a data acquisition system connected to the computer. The primary structure consists of two steel strips of 1.5 mm thickness working as leaf springs, and an aluminum plate is fixed at the top to be the primary mass. The design dimensions of the primary SDOF structure are presented in Figure 5c. A rail-train mechanism is installed (Figure 5a) on the top of the primary structure for the PID. The particle is glued to the train (which can slide over a rail) and the rail is fixed to the top of the primary structure. Using a rail-train mechanism ensures that the particle can only slide and there is no rolling motion. The experimental testing results are presented together with the simulation results using the numerical model in Sections 2 and 4.
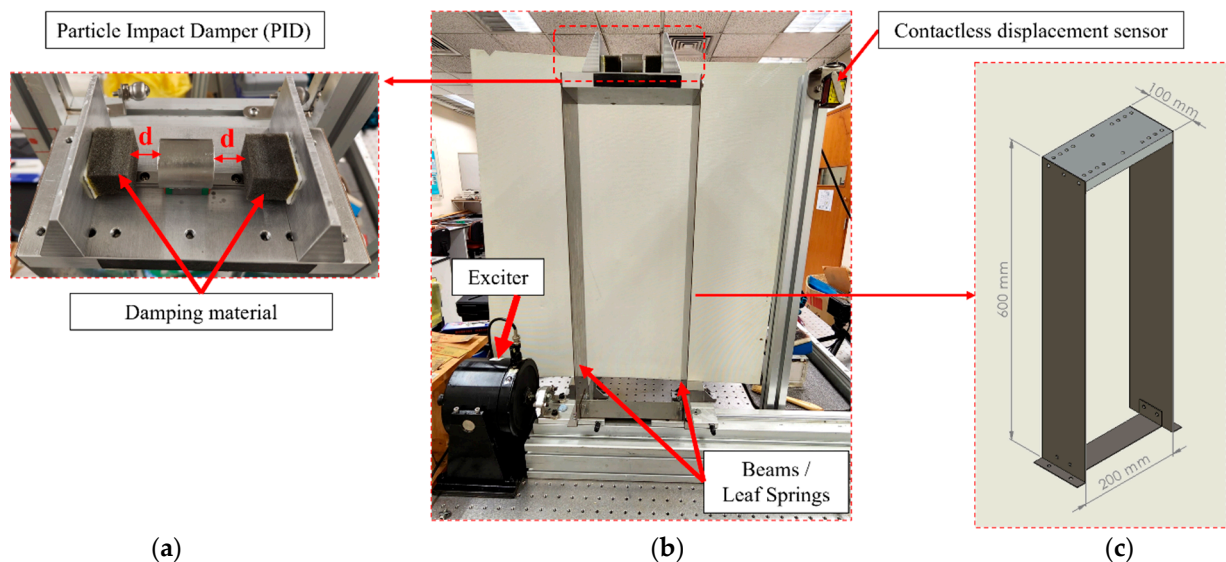
Figure 5. Schematic of (**a**) particle impact damper (PID); (**b**) experiment setup; (**c**) dimensions of the primary structure.

First of all, a free vibration test of the SDOF structure without any damper is carried out to determine the magnitude of the structural damping. The structure is provided with an initial displacement to initiate the free vibrations. The free vibration response is recorded, and the logarithmic decrement method is used to determine the internal damping magnitude of the structure. The parameters of the prototype designed for the experiments are presented in Table 2.

Furthermore, a friction damper (FD) with tunable friction is installed on the SDOF structure, as shown in Figure 6. A metal block is installed to apply friction force on one side of the primary structure and linear guide bearings are installed on the opposite side of the structure to prevent any change in the shape of the structure when friction force is applied. The normal force, in this case, can be varied by loosening or tightening the spring through the bolt and lock nut, as shown in Figure 6.

Table 2. System parameters.

System Parameters	Magnitude
Damping ratio (ζ)	0.0038
Natural frequency (f)	2.5 Hz
Mass of primary structure (M)	1605 g
Coefficient of restitution (Steel to PU Foam)	0.47
Coefficient of restitution (Steel to Aluminum)	0.82
Mass of particle	160 g
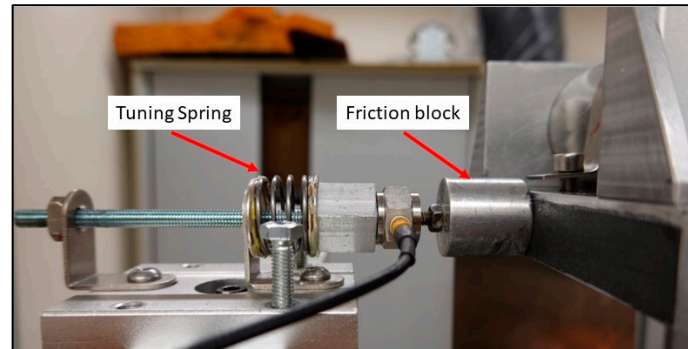
Figure 6. A prototype of a tunable friction damper (FD) attached to the PID.

4. Results for SDOF Structure

In this section, the results obtained from the numerical simulations and experiments are discussed. A sinusoidal ground motion at the base of the SDOF structure is used to excite the structure during the experiments. It is observed that the PID operates with respect to time, and that damping may vary over the time domain. The time–domain response of the primary mass shows that the amplitude increases initially due to no impacts, and then a steady-state amplitude can be observed after the first peak when there are consistent impacts. Therefore, general frequency sweep tests are invalid on the PID unless it is ensured that the system vibrates for a sufficient number of cycles at each excitation frequency. Therefore, it is challenging to determine a frequency response curve of the structure with the PID. To accurately measure the frequency response, the experiments are conducted over a set of excitation frequencies around the natural frequency of the primary mass separately. After that, the steady-state amplitude at each excitation frequency is measured and the data are combined for all frequencies to form a frequency response. The experiments are performed on the SDOF primary structure respectively with the PID only, the FD only, and the PID + FD.

4.1. Particle Impact Damper (PID)

In this section, the performance of the PID on a single-degree-of-freedom structure is tested numerically and validated with experiments. The length of the cavity of the PID can be set at 15 mm, 45 mm, and 75 mm respectively, in the experiments. The numerical simulations are performed with the same parameters used in the experiments to validate the accuracy of the numerical model.

The frequency response of the primary system determined from the experiments and simulations is shown in Figure 7. A smaller clearance ($d = 7.5$ mm) leads to lower damping as there is not enough space for the particle to gather momentum before impact, as shown in Figure 7a. On the other hand, increasing the clearance magnitude in the PID design improves the damping. Figure 7c shows that the X/Z is minimum at resonance frequency when the PID with $d = 35.5$ mm is tested. These results show that there are various nonlinear phenomena present in the PID, leading to contradicting opinions. It is one of the reasons that an optimal design method for the PID is not yet available.
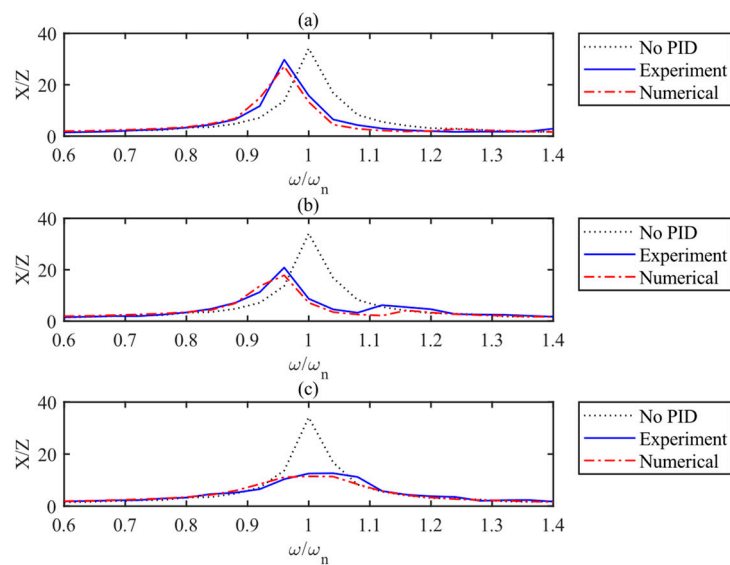
Figure 7. Simulated and measured frequency response of the primary structure: (**a**) *d* = 7.5 mm; (**b**) *d* = 22.5 mm; (**c**) *d* = 37.5 mm.

Furthermore, the effect of the coefficient of restitution is analyzed on the damping performance by changing the impact surfaces to vary the COR magnitude, as shown in Figure 8. This reveals that increasing the coefficient of restitution degrades the PID performance due to the impacts with better momentum exchange but less energy dissipation. On the other hand, the larger clearance magnitude may result in non-uniform displacement of the primary structure leading to other problems relating to structural integrity. Hence, the results show that there are nonlinear relationships with the design parameters as well.
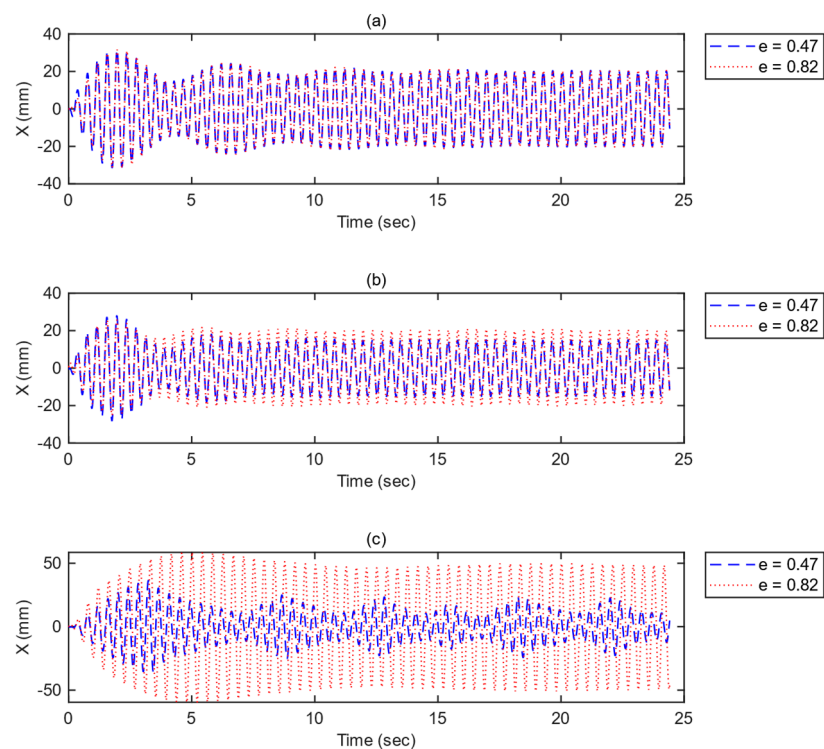
Figure 8. Measured displacement response of the primary structure at resonance with different coefficients of restitution in PID (**a**) *d* = 7.5 mm; (**b**) *d* = 22.5 mm; (**c**) *d* = 37.5 mm.

4.2. Friction Damper (FD)

In this section, the role of the friction damper (FD) in the resonant vibration of the SDOF structure is analyzed. Assuming no PID in Figure 1, the equation of motion of the SDOF structure with only the friction damper (i.e., $c = 0$) can be written as

$$M\ddot{x} + F_f \text{sgn}(\dot{x} - \dot{z}) + k(x - z) = 0 \tag{10}$$

Here, $F_f = \mu_e F_N$ is the friction force, μ_e is the coefficient of friction, and F_N is the normal force of the primary structure. A new variable friction force ratio is defined to compare the effect of external friction on the dynamic response. Friction force ratio γ_F is the ratio of friction force to excitation force, defined as

$$\gamma_F = \frac{\mu_e F_N}{kZ} \tag{11}$$

The dynamic response of the system for a finite time with different magnitudes of γ_F is recorded over a range of excitation frequencies. The plot shows the response of the SDOF structure with the FD, as shown in Figure 9.
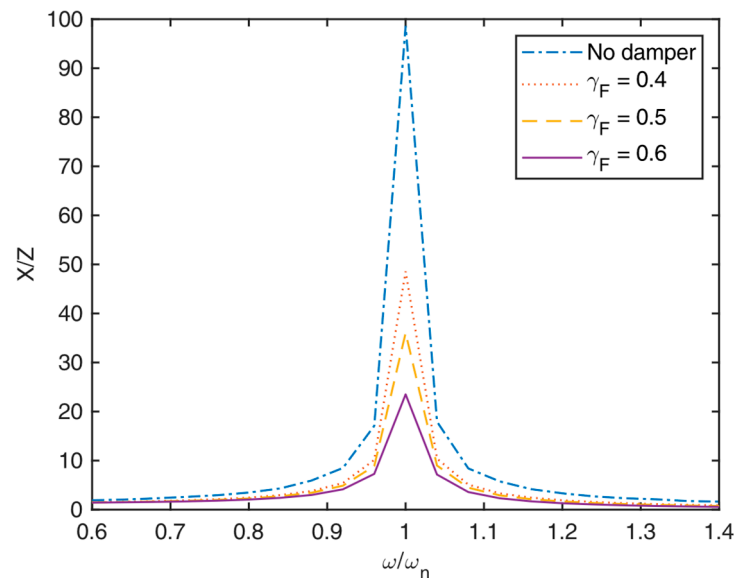
Figure 9. Simulated displacement response of the SDOF structure with FD only at different friction force ratios.

It is understood that using a sole friction damper cannot suppress the vibration amplitude efficiently at resonance, as proved by Luca et al. [48]. Furthermore, Levitan et al. [49] presented the analytical form for a single-degree-of-freedom structure with Coulomb friction under base excitations, and it was validated that the friction damper alone could not suppress the resonant vibration amplitude. Levitan shows that a structure can exhibit a harmonic response if a friction force is relatively smaller; however, a large friction force may lead to a discontinuous motion of the primary structure. Similarly, Min et al. [50] derive a solution for a friction damper at resonance; however, it is concluded that the structure cannot exhibit a steady-state response at resonance. Although friction dampers are very capable of producing a large friction force, a large friction force brings various challenges to a dynamic structure. When two masses rub against each other with a large friction force, higher temperature and excessive wearing raise questions about the reliability of the dynamic structure and damping system [51]. In addition, a large friction force is very complicated to control and it does not remain constant as the rise in temperature and material wearing/removal may alter the contact surfaces [52]. FDs have limited applications in structural vibration control due to reasons such as the stick-slip phenomenon and

nonlinear damping force, affecting the stability of the structure and leading to discomfort for living beings in the area [53]. Considering the theory of the structure with the friction damper under base excitation [54], the expression of the relative steady-state response of the primary structure under base excitation with friction damper may be written as (Appendix A)

$$\frac{A}{Z} = \left(\frac{\left(n^2\right)^2 - \left(\frac{4\mu_e N_M}{\pi k Z}\right)^2}{\left(1 - n^2\right)^2} \right)^{\frac{1}{2}} \tag{12}$$

Here, $A = X - Z$, and $n = \frac{\omega}{\omega_n}$ is the frequency ratio. Equation (12) demonstrates that the solution of this equation at resonance i.e., $(n = 1)$ becomes infinite with any magnitude of the friction force. This shows that the friction damper alone is not sufficient to suppress the vibration amplitude at resonance.

Experiments are performed with different extensions of the spring in the FD to alter the normal force applied to the primary mass. The normal force depends on the stiffness of the spring and the change in its length, as $(F_N = k_s \Delta s)$. Here, k_s is the stiffness of the spring, and $\Delta s = s_0 - s$ is the change in the length of the spring. The coefficient of external friction (μ_e) and spring stiffness (k_s) is interpreted as a constant; therefore, a change in the length of the spring changes the friction force. First of all, the spring is stretched until the metallic block is very close to the primary mass and the extension of the spring is measured, which is regarded as the zero reading. Afterwards, the spring is expanded further by loosening the nut to increase the normal force in the FD, leading to a larger friction force. The displacement response of the primary structure with different compressions of the spring in the FD is plotted in Figure 10. It can be observed that the resonant vibration amplitude reduces by increasing the deflection Δs of the spring, as shown in Figure 10. In the comparison of Figures 9 and 10, the curve of $\gamma_F = 0.6$ in Figure 9 has a similar peak value of X/Z about 20 to the curve of the FD $\Delta s = 3$mm. The experimental result validates the numerical results as increasing the friction force can reduce the vibration peak at resonance in forced vibrations. However, the vibration peak is still high even at $\gamma_F = 0.6$ which is quite close to the theoretical limit of $\pi/4$. Therefore, the FD alone is not effective in suppressing the resonant vibration of the SDOF primary system.
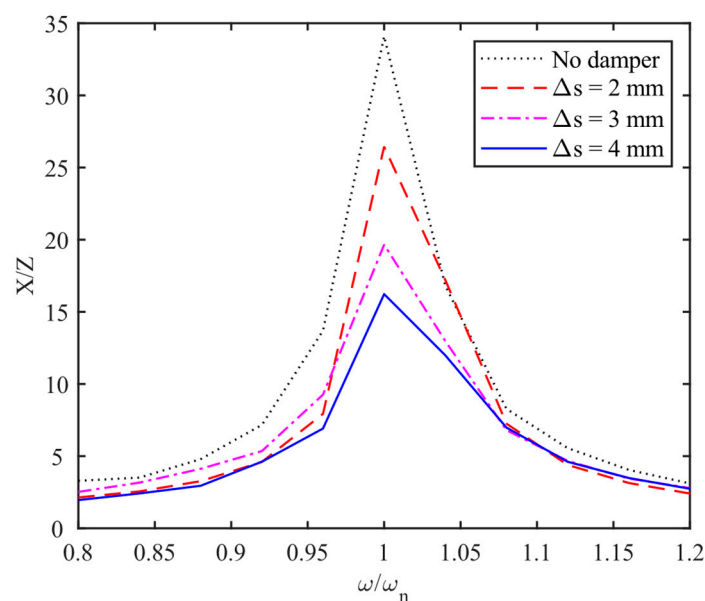
Figure 10. Measured frequency response of the primary structure with FD only at different compressions of the tuning compression spring in Figure 6.

4.3. Hybrid Damper (PID + FD)

The numerical model for a combined hybrid damper (PID + FD) proposed in Section 2 is simulated over various possible combinations of friction force ratio γ_F of the FD and relative length of the cavity d/Z of the PID to determine the steady-state displacement response of the primary structure. After that, a programme written in MATLAB software gathers this huge dataset to calculate the displacement response on each design combination at resonance. The contour plot with the 2-D dataset of resonant vibration amplitude with respect to the clearance d and friction ratio γ_F is shown in Figure 11.
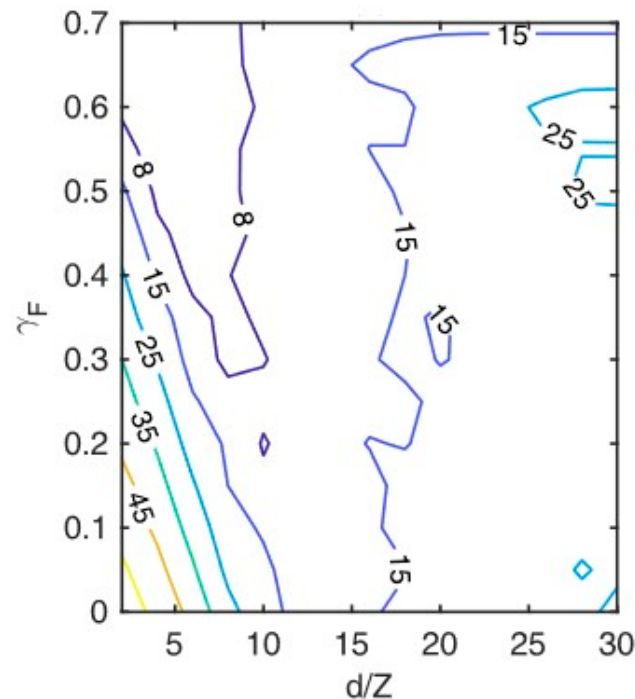
Figure 11. Contours of numerical steady-state vibration amplitude ratio (X/Z) of the SDOF structure at resonance using the proposed hybrid damper at different γ_F and d/Z.

Additionally, experiments are performed for the proposed hybrid damper consisting of a PID and FD mounted on the SDOF structure. The displacement response of the primary structure is recorded with different friction forces and clearance d of the PID. PU cushions are installed in the PID to provide soft impact effects. The displacement response of the primary structure with different spring deflections Δs of the spring in the FD and clearance d in the PID is shown in Figure 12.

The minimum resonant vibration amplitude $X/Z = 5.46$ is achieved with $d = 7.5$ mm, as shown in Table 3. The proposed hybrid damper reduces the resonant vibration amplitude by 66% in comparison to using the FD only and 43% in comparison to using the PID only with $d = 22.5$ mm.
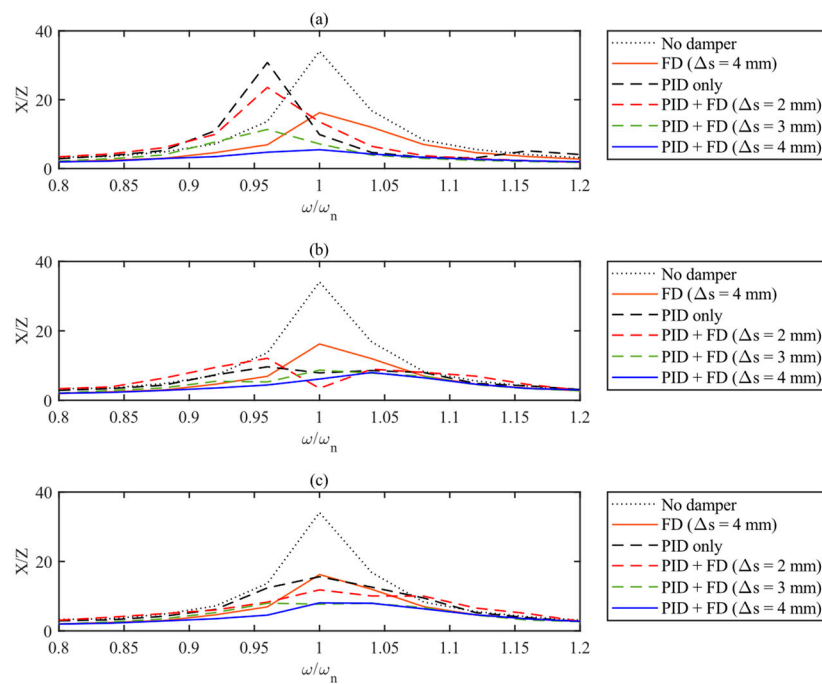
Figure 12. Measured vibration amplitudes of the primary system with different lengths of the cavity of PID (**a**) $d = 7.5$ mm. $(d/Z \approx 5)$; (**b**) $d = 22.5$ mm $(d/Z \approx 10)$; (**c**) $d = 37.5$ mm $(d/Z \approx 15)$.

Table 3. Dimensionless maximum vibration amplitude. X/Z with different dampers.

	$d = 7.5$ mm	$d = 22.5$ mm	$d = 37.5$ mm
PID only	29.73	9.64	15.06
FD only ($\Delta s = 4$ mm)	16.22	16.22	16.22
Hybrid (PID + FD)	5.46	7.99	8.06

4.4. Comparison with an Optimally Tuned Mass Damper

A traditional tuned mass damper (TMD) is a passive vibration-absorbing device, as shown in Figure 13. The TMD is a widely researched vibration absorber, resulting in considerable knowledge of analytical methods for its optimal design for maximum vibration suppression. The TMD is usually pre-tuned to the natural frequency of the primary mass; therefore, it is only effective for that frequency. In addition to being highly effective in theory, the TMD is not widely used in vast application scenarios. That is because of the challenges in practice, especially related to the precise damping requirements for the secondary mass in the TMD.
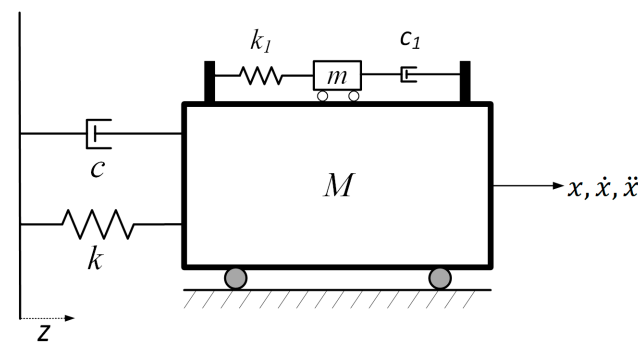
Figure 13. Schematic model of tuned mass damper (TMD).

The response of the primary structure with a TMD can be derived as [55]

$$\left|\frac{X}{X_{st}}\right| = \left|\frac{X}{Z}\right| = \sqrt{\frac{(\gamma^2 - \lambda^2)^2 + (2\gamma\lambda\zeta)^2}{[(1-\lambda^2)(\gamma^2 - \lambda^2) - \mu_1\gamma^2\lambda^2]^2 + [2\gamma\lambda\zeta(1 - \lambda^2 - \mu_1\lambda^2)]^2}} \tag{13}$$

Here, $\mu_1 = m/M$, $\gamma = \omega_a/\omega_n$, $\omega_a = \sqrt{(k_1/m)}$ and $\omega_n = \sqrt{k/M}$), $\lambda = \omega/\omega_n$, $\zeta = c/(2\sqrt{mk_1})$, and X is the vibration amplitude of the primary structure. The optimal parameters for a tuned mass damper are derived from the following equations

$$\gamma_{opt} = \frac{1}{1 + \mu_1} \tag{14}$$

$$\zeta_{opt} = \sqrt{\frac{3\mu_1}{8(1+\mu_1)}} \tag{15}$$

The response of the primary structure with an optimized TMD with design parameters, shown in Table 4, is simulated and compared with the proposed hybrid damper, as shown in Figure 14. The traditional tuned mass damper is effective at resonance; however, it requires precise tuning of the damping coefficient for its optimum function. The tuning range is usually very small and it becomes challenging to identify or design a damper with the required damping coefficient. If the damping coefficient is not accurate, the TMD can perform negatively. Additionally, the effectiveness of a tuned mass damper is determined by the actual weight that can be practically placed on top of the primary structure.

Table 4. Optimal design parameters for the comparison of TMD and proposed hybrid damper.

TMD		
Mass ratio (μ_1)	Optimal frequency ratio (γ_{opt})	Optimal damping ratio (ζ_{opt})
0.1	0.9091	0.1679
Hybrid Damper (PID + FD)			
Mass ratio (μ)	Relative clearance (d/Z)	Coefficient of restitution (e)	Spring compression (Δs)
0.1	5	0.47	4 mm
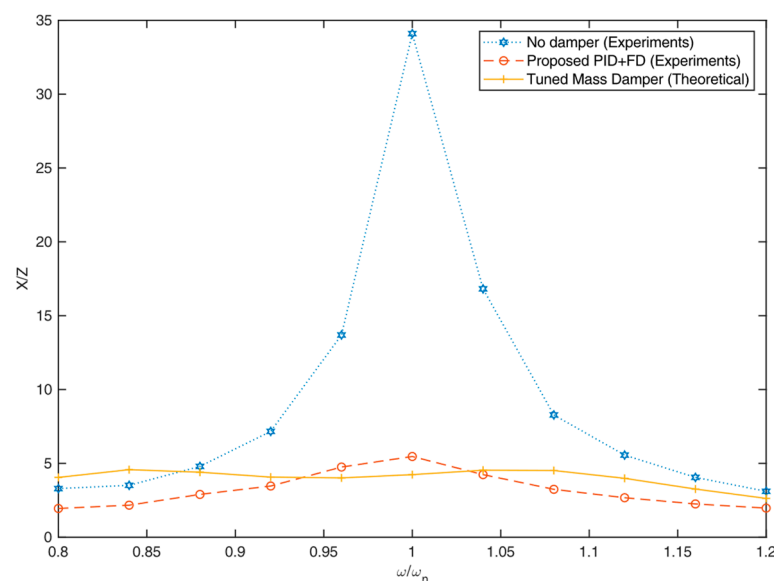
Figure 14. Comparison of the proposed hybrid damper with traditional TMD (mass ratio = 0.1).

The results show that the proposed hybrid damper (PID + FD) performs close to the optimally tuned TMD, as shown in Figure 14. It can be observed that the TMD has a smaller resonance amplitude compared with the proposed hybrid damper; however, the proposed damper shows effectiveness over a wider frequency range. In addition, the proposed damper is easier to design compared with the TMD and can perform comparably to the TMD. The proposed hybrid damper can become an alternative to the TMD for passive vibration control applications where the application of TMD is costly and challenging.

5. Conclusions

A hybrid particle impact damper (PID) combined with a Coulomb friction damper (FD) is proposed and analyzed both numerically and experimentally. The FD is found to be ineffective to suppress the resonant vibration of the primary system, and the PID has the disadvantage of a low damping-to-mass ratio. However, the proposed hybrid damper (PID + FD) is proven to be highly effective in suppressing resonant structural vibration. A theoretical model of the proposed hybrid damper is built and tested numerically on a single-degree-of-freedom (SDOF) structure. The predicted results are validated by experimental tests on a prototype of the proposed damper. A parametric analysis of the proposed hybrid damper has been performed and the optimal design combination of the PID and FD is derived numerically and validated by experiments. The proposed hybrid damper can reduce the maximum vibration amplitude of the SDOF primary structure by 66% more than using the FD only and 43% more than using the PID only.

The proposed hybrid damper can achieve a similar vibration suppression performance to the optimum tuned mass damper (TMD) of the same mass ratio. Furthermore, the proposed hybrid damper is proved to be effective over a wide range of excitation frequencies. In comparison to the TMD, the proposed hybrid damper does not require an optimally tuned natural frequency and damping and therefore it does not have the detuning problem of TMD. Additionally, random earthquake excitation data are used to compare the performance of the studied dampers. The results show that the proposed hybrid damper has significantly better damping than the TMD due to its wide frequency band. The proposed hybrid damper lowers the maximum vibration amplitude by about 46% during the earthquake compared to the TMD, as shown in Appendix B. The proposed damper may be used as a better alternative to the TMD in passive vibration control.

Nomenclature

Symbols

$\ddot{x}$	Acceleration of primary structure; m/s^2
$\ddot{y}$	Acceleration of particle; m/s^2
Z	Amplitude of support motion; m
d	Clearance; m
e	Coefficient of restitution
c	Damping coefficient; Ns/m
z	Displacement of support; m
y	Displacement of particle; m
x	Displacement of primary structure; m
$F(t)$	Excitation force; N
x_0	Initial position of primary structure; m
y_0	Initial position of particle; m
$\dot{x}_0$	Initial velocity of primary structure; m/s
$\dot{y}_0$	Initial velocity of particle; m/s
M	Mass of primary structure; kg
m	Mass of primary structure; kg
k	Spring constant; N/m
$\dot{z}$	Velocity of support; m/s
$\dot{y}$	Velocity of particle; m/s
$\dot{x}$	Velocity of primary structure; m/s
$\dot{y}_n^+$	Velocity of particle after nth impact; m/s
$\dot{y}_n^-$	Velocity of particle before nth impact; m/s
$\dot{x}_n^+$	Velocity of primary structure after nth impact; m/s
$\dot{x}_n^-$	Velocity of primary structure before nth impact; m/s

Greek Symbols

μ_e	Coefficient of friction (external)
μ_i	Coefficient of friction (internal)
ω	Frequency of excitation force; rad/s
γ_F	Friction to excitation force amplitude ratio
ω_n	Natural frequency of primary structure; rad/s
β	Mass ratio

Abbreviations

PID	Particle impact damper
RMS	Root mean square
FD	Friction damper
SDOF	Single degree of freedom

Appendix A. Steady-State Response of an SDOF Structure with Friction Damper under Harmonic Base Excitations

Considering a single-degree-of-freedom structure excited by the harmonic motion of the base, as shown in Figure A1 the structure is damped with a friction damper, where the friction damper is connected to the moving base as well.
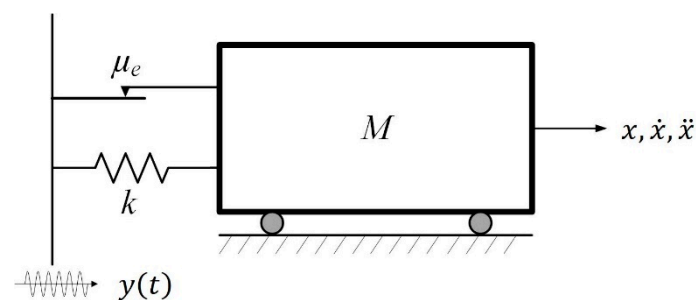
Figure A1. A single-degree-of-freedom system with friction damper.

The equation of motion of the presented system might be written as

$$M\ddot{x} + k(x - y) + \mu_e N_M \text{sgn}(\dot{x} - \dot{y}) = 0 \tag{A1}$$

Here, μ_e is the coefficient of friction, $N_M = Mg$ is the normal force of the mass M, and sgn is the signum function which is defined as

$$\text{sgn}(\dot{x} - \dot{y}) = \begin{cases} -1 \text{ if } \dot{x} - \dot{y} < 0 \\ 0 \text{ if } \dot{x} - \dot{y} = 0 \\ 1 \text{ if } \dot{x} - \dot{y} > 0 \end{cases} \tag{A2}$$

The analytical solution of Equation (A1) is difficult to achieve due to the nonlinear expressions. However, the friction damper can be assumed as an equivalent viscous damper (c_{eq}) to formulate an approximate analytical expression.

To find the equivalent viscous damping coefficient, we equate the energy dissipated by friction and the energy dissipated by an equivalent viscous damper. The energy dissipated by the friction damper in a full cycle of vibration is calculated as

$$\Delta W = 4\mu_e N_M (X - Y) \tag{A3}$$

Here, $(X - Y)$ is the relative displacement amplitude of vibration. The energy dissipated by an equivalent viscous damper in a full cycle can be determined as

$$\Delta W = \pi c_{eq} \omega (X - Y)^2 \tag{A4}$$

Here, ω is the excitation frequency. By equating Equations (A3) and (A4), we obtain

$$c_{eq} = \frac{4\mu_e N_M}{\pi\omega(X - Y)} \tag{A5}$$

Equation (A1) can be changed to

$$M\ddot{x} + c_{eq}(\dot{x} - \dot{y}) + k(x - y) = 0 \tag{A6}$$

If we consider the motion of the mass (M) relative to the base motion, we obtain

$$M\ddot{z} + c_{eq}(\dot{z}) + kz = M\ddot{y} \tag{A7}$$

Here, $z = (x - y)$. If the base has harmonic motion i.e $(y = Y\sin(\omega t))$, where Y is the amplitude of base motion. Equation (A7) is rearranged as

$$M\ddot{z} + c_{eq}\dot{z} + kz = M\omega^2 Y\sin(\omega t) \tag{A8}$$

The steady-state solution of Equation (8) is given by

$$Z = \frac{M\omega^2 Y}{\left((k - m\omega^2)^2 + (c\omega)^2\right)^{\frac{1}{2}}} \tag{A9}$$

Or

$$Z = \frac{Yn^2}{\left((1 - n^2)^2 + (2\zeta_{eq}n)^2\right)^{\frac{1}{2}}} \tag{A10}$$

Here, $n = \omega/\omega_n$ is the frequency ratio, and $\zeta_{eq} = \frac{c_{eq}}{c_c}$ is the equivalent damping ratio, giving

$$\zeta_{eq} = \frac{c_{eq}}{c_c} = \frac{\frac{4\mu_e N_M}{\pi\omega Z}}{2M\omega_n} = \frac{4\mu_e N_M}{2\pi M\omega_n \omega Z} \tag{A11}$$

and $Z = X - Y$, substituting Equation (A11) into Equation (A10) gives

$$Z = \frac{Yn^2}{\left((1-n^2)^2 + \left(\left(\frac{4\mu_e N_M}{\pi k Z}\right)\right)^2\right)^{\frac{1}{2}}} \tag{A12}$$

Squaring both sides and rearranging gives

$$Z^2\left(\left(1-n^2\right)^2 + \left(\left(\frac{4\mu_e N_M}{\pi k Z}\right)\right)^2\right) = \left(Yn^2\right)^2 \tag{A13}$$

$$Z^2\left(1-n^2\right)^2 + \left(\frac{4\mu_e N_M}{\pi k}\right)^2 = \left(Yn^2\right)^2 \tag{A14}$$

$$Z^2\left(1-n^2\right)^2 = \left(Yn^2\right)^2 - \left(\frac{4\mu_e N_M}{\pi k}\right)^2 \tag{A15}$$

Multiplying with $\frac{1}{Y^2}$ gives

$$\frac{1}{Y^2}\left(Z^2\left(1-n^2\right)^2\right) = \frac{1}{Y^2}\left(\left(Yn^2\right)^2 - \left(\frac{4\mu_e N_M}{\pi k}\right)^2\right) \tag{A16}$$

$$\frac{Z^2}{Y^2}\left(\left(1-n^2\right)^2\right) = \frac{Y^2 n^4}{Y^2} - \left(\left(\frac{4\mu_e N_M}{\pi k}\right)^2\right)\frac{1}{Y^2} \tag{A17}$$

$$\frac{Z^2}{Y^2}\left(\left(1-n^2\right)^2\right) = n^4 - \left(\left(\frac{4\mu_e N_M}{\pi k Y}\right)^2\right) \tag{A18}$$

$$\frac{Z^2}{Y^2} = \frac{n^4 - \left(\frac{4\mu_e N_M}{\pi k Y}\right)^2}{(1-n^2)^2} \tag{A19}$$

Taking the square root of both sides gives

$$\frac{Z}{Y} = \left(\frac{\left(n^2\right)^2 - \left(\frac{4\mu_e N_M}{\pi k Y}\right)^2}{(1-n^2)^2}\right)^{\frac{1}{2}} \tag{A20}$$

Equation (A13) is the steady-state response of a single-degree-of-freedom structure with friction damper under harmonic base excitations.

Appendix B. Random Excitation Case

The proposed hybrid damper is designed and tested under harmonic excitations in previous sections. However, the excitation in practice is sometimes random, such as an earthquake. Considering the potential applications of the proposed hybrid damper in an earthquake, the model is tested under random earthquake data. The earthquake input is extracted from the built-in MATLAB example data "quake", which contains earthquake data from the Loma Prieta earthquake in the Santa Cruz Mountains on 17 October 1989. The test under earthquake data is performed numerically and compared with the optimally tuned mass damper with a similar mass ratio under the same excitation conditions.

Figure A2 shows a random earthquake example case for the proposed hybrid damper compared with the other dampers tested in this article. The results show that the proposed damper provides better damping to the SDOF under random excitation. The proposed damper performs better in this case due to its wide frequency band, unlike the TMD which is tuned for one frequency. Random excitations are generally with a range of excitation

frequencies. Regarding the nature of the article, this could be an interesting topic to study in the future.
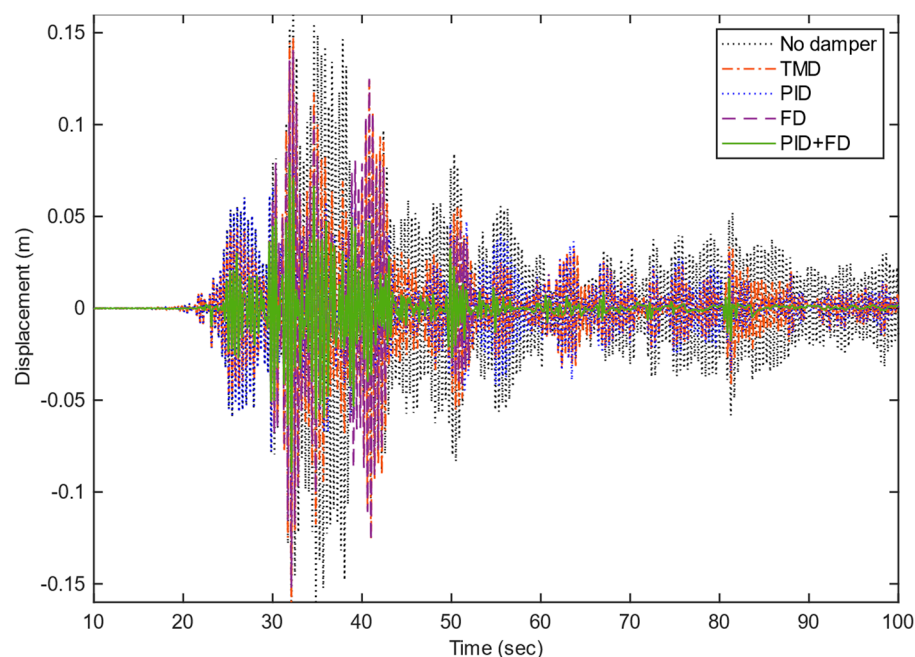
Figure A2. Comparison of the response of the SDOF structure under earthquake excitation with different dampers.

Table A1 presents the maximum and RMS amplitude of the primary structure under earthquake excitation with different dampers. The RMS amplitude represents the overall performance of the damper during the whole excitation period and shows the effectiveness of the damper over a longer duration. Comparing the maximum and RMS amplitude of the structure with different dampers, the proposed hybrid damper shows the best vibration suppression. The proposed hybrid damper reduces the maximum vibration amplitude by 46% compared to the TMD.

Table A1. Maximum and RMS amplitude of primary structure under earthquake excitation with different dampers.

	No Damper	TMD	PID	FD	PID + FD
Maximum amplitude (m)	0.1671	0.1473	0.0851	0.1400	0.0790
RMS amplitude (m)	0.0335	0.0238	0.0168	0.0200	0.0106

References

1. Mrad, C.; Titirla, M.D.; Larbi, W. Comparison of Strengthening Solutions with Optimized Passive Energy Dissipation Systems in Symmetric Buildings. *Appl. Sci.* **2021**, *11*, 10103. [CrossRef]
2. Zhang, J.; Zhu, Y.; Tu, J.; Li, Z.; Wang, Q. Development and Vibration Control of Frequency Adjustable Tuned Mass Damper Based on Magnetorheological Elastomer. *Materials* **2022**, *15*, 1829. [CrossRef] [PubMed]
3. Yang, F.; Sedaghati, R.; Esmailzadeh, E. Vibration suppression of structures using tuned mass damper technology: A state-of-the-art review. *J. Vib. Control* **2022**, *28*, 812–836. [CrossRef]
4. Lin, G.L.; Lin, C.C.; Chen, B.C.; Soong, T.T. Vibration control performance of tuned mass dampers with resettable variable stiffness. *Eng. Struct.* **2015**, *83*, 187–197. [CrossRef]
5. Werkle, H.; Butz, C.; Tatar, R. Effectiveness of "Detuned" TMD's for Beam-Like Footbridges. *Adv. Struct. Eng.* **2013**, *16*, 21–31. [CrossRef]
6. Taflanidis, A.A.; Angefides, D.C.; Scruggs, J.T. Simulation-based robust design of mass dampers for response mitigation of tension leg platforms. *Eng. Struct.* **2009**, *31*, 847–857. [CrossRef]
7. Marano, G.C.; Greco, R. Robust Optimum Design of Tuned Mass Dampers for High-Rise Buildings under Moderate Earthquakes. *Struct. Des. Tall Spec. Build.* **2009**, *18*, 823–838. [CrossRef]

8.   Ueng, J.M.; Lin, C.C.; Wang, J.F. Practical design issues of tuned mass dampers for torsionally coupled buildings under earthquake loadings. *Struct. Des. Tall Spec. Build.* **2008**, *17*, 133–165. [CrossRef]

9.   Wang, J.F.; Lin, C.C.; Chen, B.L. Vibration suppression for high-speed railway bridges using tuned mass dampers. *Int. J. Solids Struct.* **2003**, *40*, 465–491. [CrossRef]

10.   Rana, R.; Soong, T.T. Parametric study and simplified design of tuned mass dampers. *Eng. Struct.* **1998**, *20*, 193–204. [CrossRef]

11.   Wang, Q.; Dan, D. A simplified modeling method for multi-particle damper: Validation and application in energy dissipation analysis. *J. Sound Vib.* **2022**, *517*, 116528. [CrossRef]

12.   Friend, R.D.; Kinra, V.K. Particle impact damping. *J. Sound Vib.* **2000**, *233*, 93–118. [CrossRef]

13.   Lu, Z.; Wang, Z.X.; Masri, S.F.; Lu, X.L. Particle impact dampers: Past, present, and future. *Struct. Control Health Monit.* **2018**, *25*, e2058. [CrossRef]

14.   Lu, Z.; Huang, B.; Wang, Z.X.; Zhou, Y. Experimental Comparison of Dynamic Behavior of Structures with a Particle Damper and a Tuned Mass Damper. *J. Struct. Eng.* **2018**, *144*, 04018211. [CrossRef]

15.   Tomlinson, G.R.; Pritchard, D.; Wareing, R. Damping characteristics of particle dampers—Some preliminary results. *Proc. Inst. Mech. Eng. Part C J. Mech. Eng. Sci.* **2001**, *215*, 253–257. [CrossRef]

16.   Lu, Z.; Li, K.; Zhou, Y. Comparative Studies on Structures with a Tuned Mass Damper and a Particle Damper. *J. Aerosp. Eng.* **2018**, *31*, 04018090. [CrossRef]

17.   Saeki, M. Impact damping with granular materials in a horizontally vibrating system. *J. Sound Vib.* **2002**, *251*, 153–161. [CrossRef]

18.   Gagnon, L.; Morandini, M.; Ghiringhelli, G.L. A review of particle damping modeling and testing. *J. Sound Vib.* **2019**, *459*, 114865. [CrossRef]

19.   Xu, Z.W.; Wang, M.Y.; Chen, T.N. Particle damping for passive vibration suppression: Numerical modelling and experimental investigation. *J. Sound Vib.* **2005**, *279*, 1097–1120. [CrossRef]

20.   Ibrahim, R.A. *Vibro-Impact Dynamics: Modeling, Mapping and Applications*; Springer: Berlin/Heidelberg, Germany, 2009; Volume 43.

21.   Lu, Z.; Lu, X.L.; Jiang, H.J.; Masri, S.F. Discrete element method simulation and experimental validation of particle damper system. *Eng. Comput.* **2014**, *31*, 810–823. [CrossRef]

22.   Michon, G.; Almajid, A.; Aridon, G. Soft hollow particle damping identification in honeycomb structures. *J. Sound Vib.* **2013**, *332*, 536–544. [CrossRef]

23.   Olson, S.E. An analytical particle damping model. *J. Sound Vib.* **2003**, *264*, 1155–1166. [CrossRef]

24.   Bapat, C.N.; Sankar, S. Single Unit Impact Damper in Free and Forced Vibration. *J. Sound Vib.* **1985**, *99*, 85–94. [CrossRef]

25.   Marhadi, K.S.; Kinra, V.K. Particle impact damping: Effect of mass ratio, material, and shape. *J. Sound Vib.* **2005**, *283*, 433–448. [CrossRef]

26.   Papalou, A.; Masri, S.F. An experimental investigation of particle dampers under harmonic excitation. *J. Vib. Control* **1997**, *4*, 361–379. [CrossRef]

27.   Cheng, C.C.; Wang, J.Y. Free vibration analysis of a resilient impact damper. *Int. J. Mech. Sci.* **2003**, *45*, 589–604. [CrossRef]

28.   Li, X.W.; Yang, Y.; Shi, W.X. Study on the Damping Effect of Particle Dampers considering Different Surface Properties. *Shock Vib.* **2019**, *2019*, 8293654. [CrossRef]

29.   Veeramuthuvel, P.; Sairajan, K.K.; Shankar, K. Vibration suppression of printed circuit boards using an external particle damper. *J. Sound Vib.* **2016**, *366*, 98–116. [CrossRef]

30.   Chen, J.L.; Georgakis, C.T. Tuned rolling-ball dampers for vibration control in wind turbines. *J. Sound Vib.* **2013**, *332*, 5271–5282. [CrossRef]

31.   Shah, B.M.; Pillet, D.; Bai, X.M.; Keer, L.M.; Wang, Q.J.; Snurr, R.Q. Construction and characterization of a particle-based thrust damping system. *J. Sound Vib.* **2009**, *326*, 489–502. [CrossRef]

32.   Du, Y.C.; Wang, S.L. Modeling the fine particle impact damper. *Int. J. Mech. Sci.* **2010**, *52*, 1015–1022. [CrossRef]

33.   Zhang, R.L.; Wu, C.J.; Zhang, Y.T. A novel technique to predict harmonic response of Particle-damping structure based on ANSYS (R) secondary development technology. *Int. J. Mech. Sci.* **2018**, *144*, 877–886. [CrossRef]

34.   Jin, J.; Yang, W.; Koh, H.I.; Park, J. Development of tuned particle impact damper for reduction of transient railway vibrations. *Appl. Acoust.* **2020**, *169*, 107487. [CrossRef]

35.   Badri, Y.; Sassi, S.; Hussein, M.; Renno, J. Experimental and numerical investigation of damping in a hybrid automotive damper combining viscous and multiple-impact mechanisms. *J. Vib. Control* **2021**, *28*, 3676–3687. [CrossRef]

36.   Titirla, M.D. A State-of-the-Art Review of Passive Energy Dissipation Systems in Steel Braces. *Buildings* **2023**, *13*, 851. [CrossRef]

37.   Gagnon, L.; Morandini, M.; Ghiringhelli, G.L. A review of friction damping modeling and testing. *Arch. Appl. Mech.* **2020**, *90*, 107–126. [CrossRef]

38.   Hartog, J.P.D. Forced vibrations with combined viscous and coulomb damping. *Lond. Edinb. Dublin Philos. Mag. J. Sci.* **2009**, *9*, 801–817. [CrossRef]

39.   Mansour, W.M.; Filho, D.R.T. Impact Dampers with Coulomb Friction. *J. Sound Vib.* **1974**, *33*, 247–265. [CrossRef]

40.   Hundal, M.S. Response of a Base Excited System with Coulomb and Viscous Friction. *J. Sound Vib.* **1979**, *64*, 371–378. [CrossRef]

41.   Ziaee, M.; Hejazi, F. Development of Non-sticking Steady-State solution for structures with hybrid damping mechanism. *Structures* **2023**, *47*, 233–245. [CrossRef]

42.   Sun, R.Q.; Wong, W.O.; Cheng, L. A tunable hybrid damper with Coulomb friction and electromagnetic shunt damping. *J. Sound Vib.* **2022**, *524*, 116778. [CrossRef]

43. Sun, R.Q.; Wong, W.O.; Cheng, L. Hybrid electromagnetic shunt damper with Coulomb friction and negative impedance converter. *Int. J. Mech. Sci.* **2022**, *230*, 107552. [CrossRef]

44. Xia, X.J.; Zheng, M.Y.; Liu, P.F.; Zhang, N.; Ning, D.H.; Du, H.P. Friction observer-based hybrid controller for a seat suspension with semi-active electromagnetic damper. *Mechatronics* **2021**, *76*, 102568. [CrossRef]

45. Atam, E. Friction Damper-Based Passive Vibration Control Assessment for Seismically-Excited Buildings Through Comparison With Active Control: A Case Study. *IEEE Access* **2019**, *7*, 4664–4675. [CrossRef]

46. Popescu, F.D.; Radu, S.M.; Kotwica, K.; Andraș, A.; Kertesz, I. Simulation of the Time Response of the ERc 1400-30/7 Bucket Wheel Excavator's Boom during the Excavation Process. *Sustainability* **2019**, *11*, 4357. [CrossRef]

47. Lu, Z.; Lu, X.L.; Masri, S.F. Studies of the performance of particle dampers under dynamic loads. *J. Sound Vib.* **2010**, *329*, 5415–5433. [CrossRef]

48. Marino, L.; Cicirello, A.; Hills, D.A. Displacement transmissibility of a Coulomb friction oscillator subject to joined base-wall motion. *Nonlinear Dyn.* **2019**, *98*, 2595–2612. [CrossRef]

49. Levitan, E.S. Forced Oscillation of a Spring-Mass System having Combined Coulomb and Viscous Damping. *J. Acoust. Soc. Am.* **1960**, *32*, 1265–1269. [CrossRef]

50. Min, K.W.; Seong, J.Y.; Kim, J. Simple design procedure of a friction damper for reducing seismic responses of a single-story structure. *Eng. Struct.* **2010**, *32*, 3539–3547. [CrossRef]

51. López, I.; Busturia, J.M.; Nijmeijer, H. Energy dissipation of a friction damper. *J. Sound Vib.* **2004**, *278*, 539–561. [CrossRef]

52. Spencer, B.F.; Nagarajaiah, S. State of the Art of Structural Control. *J. Struct. Eng.* **2003**, *129*, 845–856. [CrossRef]

53. Ding, Q.; Chen, Y. Analyzing resonant response of a system with dry friction damper using an analytical method. *J. Vib. Control* **2008**, *14*, 1111–1123. [CrossRef]

54. Jaisee, S.; Yue, F.; Ooi, Y.H. A state-of-the-art review on passive friction dampers and their applications. *Eng. Struct.* **2021**, *235*, 112022. [CrossRef]

55. Wong, W.O. Optimal design of a hysteretic vibration absorber using fixed-points theory. *J. Acoust. Soc. Am.* **2016**, *139*, 3110. [CrossRef] [PubMed]